ADVANCED FUNCTIONAL MATERIALS
www.afm-journal.de

Materials Views
www.MaterialsViews.com

Homogeneous Optical and Electronic Properties of Graphene Due to the Suppression of Multilayer Patches During CVD on Copper Foils

*Zheng Han, Amina Kimouche, Dipankar Kalita, Adrien Allain, Hadi Arjmandi-Tash, Antoine Reserbat-Plantey, Laëtitia Marty, Sébastien Pairis, Valérie Reita, Nedjma Bendiab, Johann Coraux, and Vincent Bouchiat**

A synthesis method of strictly monolayer and fully homogeneous graphene across tens of centimeter squares, by chemical vapour deposition onto standard copper foils, is presented. The growth technique involves cyclic injection of a carbon precursor separated by idle times with constant hydrogen exposure. The formation of spurious multilayer patches, which accompanies the standard growth techniques based on continuous exposure to methane, is inhibited here, in a broad range of pressure and gas composition, including in two pressure regimes which are known to yield distinctive grain morphologies (dendritic versus hexagonal). Raman spectra confirm the absence of defects within the graphene films. A mechanism for growth/suppression of the multilayer patches based on the carbon storage at defective regions is proposed. The importance of multilayer suppression is highlighted in a comparative study showing the detrimental effect of patches on the performances of graphene transistors and on the optical transparency of stacked layers. The full-layer graphene sheets are superiorly homogeneous in terms of their optical and electronic properties, and are thus suited for applications for high-density integration as well as transparent electrodes with spatially continuous optical absorbance. Graphene transistors fabricated by the pulsed CVD method exhibit room-temperature mobilities with a mean value of 5000 $cm^2 V^{-1} s^{-1}$.

1. Introduction

Emerging applications using graphene[1] as transparent and flexible electrodes or as a high mobility 2D electronic material for radiofrequency, terahertz, or opto-electronics devices all require batch and scalable production of macroscale monolayer sheets that are transferable on arbitrary substrates while showing high electronic mobility. To achieve this goal, chemical vapor deposition (CVD) of graphene on copper[2] appears as a very promising and increasingly popular production route as it fulfills the two above requirements.[3] However, graphene produced following this growth method is far from the ideal case of flat defect-free macroscopic monolayer single crystals but rather comprises diverse types of disorder, namely, mosaicity due to the presence of disoriented grains (thus presence of grain boundaries), wrinkles, and multilayered patches. All these three types of disorder are recognized as important and timely issues since they limit device engineering and applications, and shall be controlled and eventually suppressed to further promote the use of CVD-grown graphene in applications requiring homogeneity, such as high density integration.[4]

This objective has fostered considerable efforts during the last few years, leading to remarkable improvements since the seminal experiments.[2] For example, the formation of wrinkles, that hampers the electron transport,[5] may be circumvented by modifying the transfer procedure over the desired substrate.[6,7] The exploration of the growth parameter space recently allowed one to prepare millimeter-size single-crystal graphene,[10] thus to reduce the influence of grain boundaries that are known as electron scattering barriers limiting the large scale electron mobility.[8,9]

In this paper, we turn towards the study of the influence of the third type of defect found in most CVD-grown graphene, that is, the multilayer patches, whose control and reduction have been widely overlooked thus far. This type of defect is however highly detrimental for both optical and electrical properties. Multilayer patches are usually found to nucleate at the defect sites and are scattered under the monolayer graphene typically along scratches, grain boundaries, and impurities of the copper substrate. This local variation in the number of graphene layers is ubiquitous in graphene grown on copper foils and can fill up to 70% of the graphene total area (see the literature[11] and also Figure S1, Supporting Information). Several

Z. Han, A. Kimouche, D. Kalita, Dr. A. Allain, H. Arjmandi-Tash, Dr. A. Reserbat-Plantey, Dr. L. Marty, Dr. S. Pairis, Dr. V. Reita, Dr. N. Bendiab, Dr. J. Coraux, Prof. V. Bouchiat
Univ. Grenoble, Alpes, Inst. NEEL, F-38042 Grenoble France and CNRS, Inst. NEEL
F-38042 Grenoble, France
E-mail: bouchiat@grenoble.cnrs.fr

DOI: 10.1002/adfm.201301732

© 2013 WILEY-VCH Verlag GmbH & Co. KGaA, Weinheim

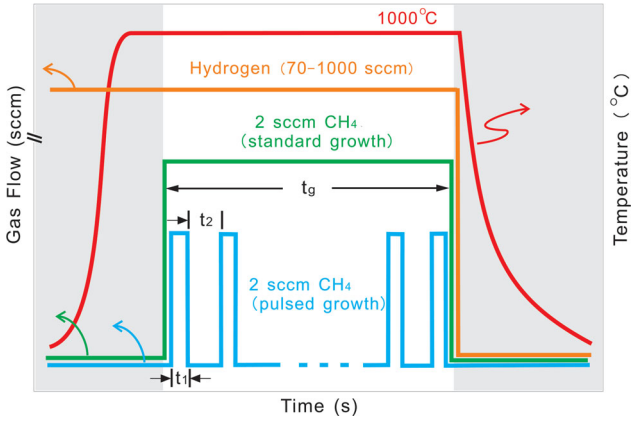

Figure 1. Process flows comparing the time evolutions of furnace temperatures and injected gases for standard-CVD (continuous) growth and the pulsed-CVD growth methods proposed in this work. Pulsed growth is characterized by carbon injection pulse time t_1 and idle time without carbon exposure t_2 and total growth time t_g.

approaches have been pursued to limit its occurrence, notably by using single-crystal Cu that has shown to suppress multilayers up to the centimeter scale.[12] However the cost of such a substrate and the stringent conditions needed for preparing it restrict its usage only to the laboratory scale. In the present work, we show that, rather than using high-quality Cu surfaces, one can achieve fully homogeneous single-layer graphene on standard copper foils by controlling the growth parameters, in a way entirely compatible with mass-production.

2. Presentation of the Pulsed CVD Growth Method

We first recall the general features of CVD graphene. Among many reported recipes,[8,10,13–19] CVD graphene domains are known to be either dendritically or hexagonally shaped. The dendritic morphology originates from the so-called diffusion-limited growth,[14,16] which leads to a fractal crystal with rough edges. On the opposite, straight-edge hexagon-shaped crystals are obtained in conditions when edge diffusion and/or preferential H_2 etching of less stable edges (non zigzag) become significant.[19,20] Even though most reported hexagonal graphene islands are obtained at the ambient pressure, by precisely tuning the flow rates of carbon and hydrogen precursors and the ratio between them, both dendritic- and hexagonal-regimes can be reached under the same total pressure (either ambient, or mbar pressure).[19] In reported recipes of CVD graphene growth on Cu, gaseous carbon source and hydrogen (sometimes together with an inert gas to tune the partial pressure of each) are usually injected in a continuous flow throughout the growth duration t_g (**Figure 1**, green curve), as it has been proposed in the seminal experiment.[2] We refer to this conventional continuous injection CVD method as "standard-CVD".

We introduce here a novel type of CVD growth of graphene that will be referred to in the following as "pulsed-CVD". It consists in exposing the catalytic substrate to the carbon precursor (methane in this work) in an intermittent fashion during the growth steps (see process flow in Figure 1). More precisely, pulsed-CVD consists in a sequence of methane injection pulses of time duration t_1 (typically a few seconds) separated by idling steps of duration t_2, during which methane injection is halted while the hydrogen flux is kept constant at the same value as that during the growth steps. We have found the optimal (in terms of multi-layer removal) sets of parameters for dendritic (t_1 = 10 s, t_2 = 50 s) and hexagonal (t_1 = 5 s, t_2 = 55 s) regimes. More experimental details such as the influence of t_1 and t_2 on the growth can be found in Figure S3, Supporting Information.

Figure 2 shows a series of scanning electron micrographs (SEM) of graphene on copper for which the growth has been stopped before reaching full Cu surface coverage in order to highlight the shape of the flakes, easing side-by-side comparison of standard- and pulsed-CVD growth for both dendritic and hexagonal regimes. In the case of the standard-CVD, multilayers

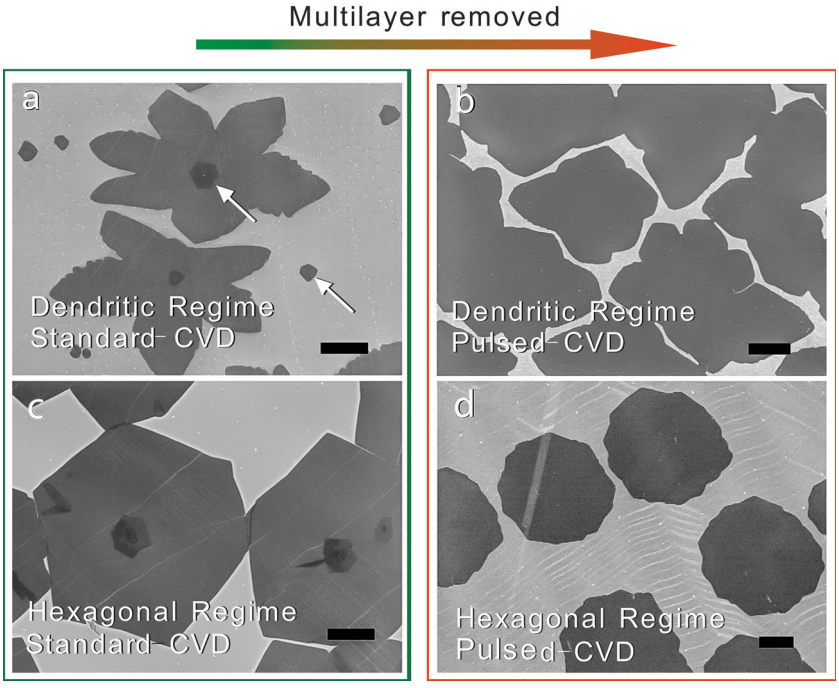

Figure 2. SEM images of raw graphene samples on Cu for which growth was interrupted before reaching full surface coverage, showing for comparison graphene grain morphology for standard-CVD growth (left column) and pulsed-CVD growth (right column). a) Dendritic growth with partial pressure 2.8 µbar CH_4, 0.1 mbar H_2, and c) hexagonal flakes morphology with partial pressure 50 µbar CH_4, 25 mbar H_2. Temperature was always kept at 1000 °C. Duration for (a) and (c) are 20 min and 5 min, respectively. For the right column, same parameters are used except for the pulsed-injection of CH_4 gas. The parameters t_1/t_2/number-of-pulses for the cases in b) and d) are 10s/50s/120 pulses, and 5s/55s/40 pulses, respectively. Arrows in a) indicate the distinctive shape of the multilayer patches. Scale bars are 10 µm.

© 2013 WILEY-VCH Verlag GmbH & Co. KGaA, Weinheim

can be clearly seen (Figure 2a,c) as reported many times, mostly occurring at the centers of the graphene grains. When the same growth conditions are used during the pulsed-CVD, no multilayer formation can be seen. Interestingly, significant modifications of grain shapes are observed for the pulsed-CVD in the hexagonal regime. The exact hexagonal shape usually found (Figure 2c) is altered, giving rise to a more rounded polygon, a shape that we attribute to be the hallmark of the pulsed CVD growth. Such multi-faceted grains result from the back-etching of graphene by hydrogen during idle time, a process known to occur preferentially at crystal corners.

The fact that multilayers show up in all standard growth regimes suggests that their formation does not depend on the growth conditions but rather relies on a process that is affected by transients. Modifying the nature of these transients during the growth was also recognized to be effective for directly acting on the graphene layer morphology, which will be further discussed in Section 4.

3. Compared Raman Spectrometry Analyses

Confocal micro-Raman mapping provides an efficient tool to assess the quality of the obtained graphene. Intensity mapping of graphene specific Raman bands, shown in **Figure 3**, was performed on two batches grown in the high-pressure regime using both standard-CVD (Figure 3a) or pulsed-CVD (Figure 3d) and subsequently transferred onto Si/SiO_2 (see Experimental Section). The defect-activated D band is uniformly very low and mostly hardly detectable except at some edges for both batches. Except for the central region of flakes grown by standard-CVD, the G and 2D bands show single Lorentzian shape and are also uniform and narrow (Figure 3g), with a full-width at half maximum (FWHM) of 18 and 30 cm^{-1} respectively, with a typical deviation of about ±2 and ±4 cm^{-1} over the surface of a single flake, respectively. These features are typical of high quality single-layer graphene.[21]

The central part of the flakes prepared by the standard-CVD exhibits non-uniform G and 2D bands, pointing to the presence of few-layer (two, three, and sometimes even more) graphene, consistent with the SEM observations (Figure 2). Such regions are not observed on the pulsed-CVD-grown graphene which shows uniform spectra like the one in light blue of Figure 3g. the intensity of G-band is increasing by a factor 2 and 3, confirming assignement of the number of layers.[21] The intensities of the 2D peak in the same central region do not follow the same linear increase and profiles show deviations from single-Lorentzian shape (green and purple dots in Figure 3c), a feature linked to the stacking order.[22] This is a strong indication that the multi-layers are randomly stacked, namely, they lead to turbostratic rather than Bernal-stacked few layer graphene.[19]

4. Multilayer Formation in Standard CVD and Their Suppression in Pulsed-CVD

To begin with, we briefly recall the concept of graphene CVD growth. Multilayer graphene formation on metal surfaces under carbon precursor exposure was already studied in the '80s[23] and was even long before recognized as poison for catalyst activity in carbon based reactions.[24,25] Indeed, during CVD growth of graphene, the metal surface serves as a catalyst, which adsorbs and dissociates carbon precursor molecules into a two-dimensional "gas" of carbon species. Nucleation of 2D carbon

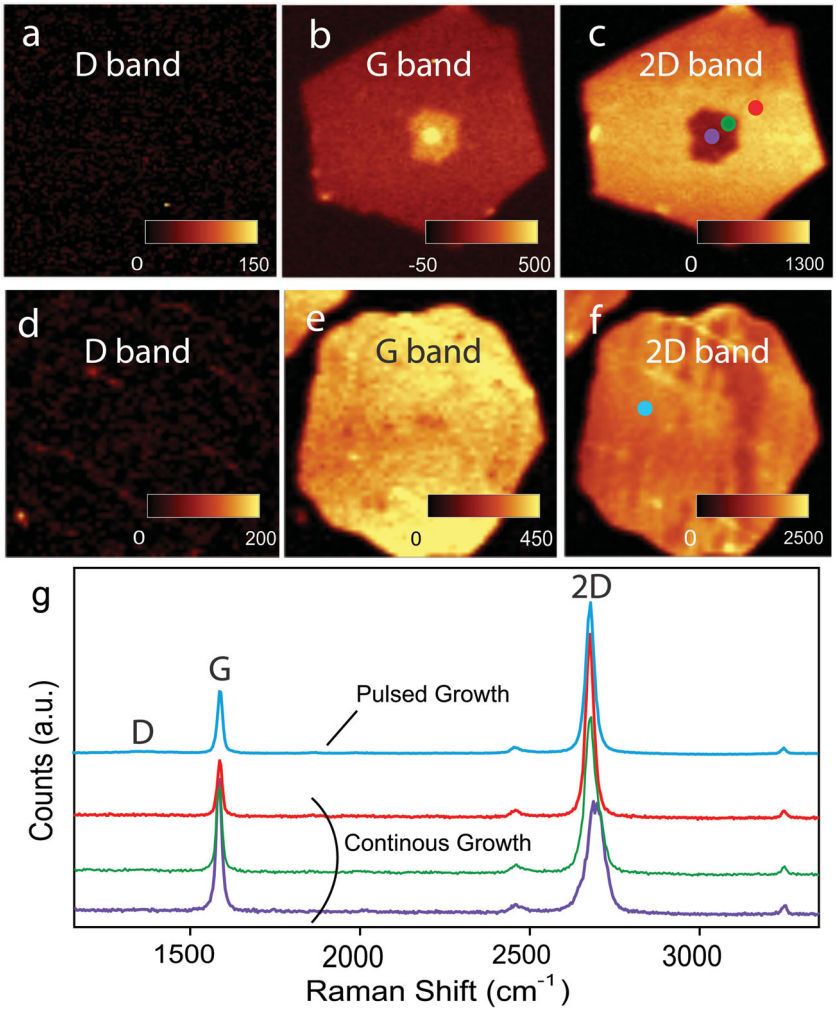

Figure 3. Intensity maps (scan area is 20 µm × 20 µm) obtained by scanning confocal micro-Raman of graphene grains obtained in the high pressure regime for a–c) continuous and d–f) pulsed growth which corresponds to samples shown in Figure 2c,d. From left to right are D, G, and 2D bands, respectively. g) Single spectra taken at dotted areas, from both top and bottom maps. All measurements are performed on graphene transferred onto standard Si/SiO_2 substrate (see Experimental Section).

© 2013 WILEY-VCH Verlag GmbH & Co. KGaA, Weinheim

"solids" (i.e., graphene nanocrystals) occurs when a threshold concentration of surface carbon atom gas is reached. However, this 2D surface-growth is valid only for metals with low carbon solubility. Otherwise, surface carbon atoms can diffuse into the metal bulk, and segregate out at surface again upon cool down for instance. When this "bulk segregation" happens underneath the already-grown graphene island, it leads to a multi-layer.[26]

Due to the low carbon solubility in Cu,[27] CVD of graphene on Cu is a surface-confined process which is self-terminated once no more catalytic surface (bare Cu) is available, that is, once a single layer of graphene covers the whole surface and passivates it.[28] The occurrence of multilayer patches in graphene prepared by CVD on Cu seems in contradiction with this common wisdom. A scenario lifting this apparent contradiction has been proposed recently, in which carbon adatoms were argued to intercalate between graphene and Cu via the edges of graphene and condense in the form of a graphene multi-layer patch at the center of the large flake.[29] However, this scenario can hardly account for the fact that multilayer regions of similar shape and size are not only observed at the center of large dendritic flakes, but also in between them (Figure 2a, indicated by arrows). We interpret this observation by invoking an alternative scenario, in which extended defects in Cu play a central role. Such defects (e.g., Cu grain boundaries) have been shown to be pathways for carbon atoms during CVD of graphene.[30] Another example was demonstrated by manually introducing scratches on Cu surface, which resulted in preferential nucleation sites for multilayer graphene.[17] It can be understood that high carbon solubility and large diffusion coefficient of carbon are at play at defects such as grain boundaries, dislocations, edges, etc. Prolonged exposure to methane at high temperature, during standard CVD, must hence lead to a carbon saturation of the defects. A carbon supersaturation at these defects during CVD, a decrease of the carbon equilibrium concentration along these defects upon cooldown, or a combination of the two, will lead to surface segregation of carbon yielding the observed multilayer graphene patches.

To confirm the "underground" formation of these patches, we used a partial liftoff technique adapted from the exfoliation technique using adhesive tape (see Figure S2, Supporting Information). We unambiguously find, consistent with previous observations,[25,26,29] that these multilayer patches are indeed capped by the surface grown layer (Figure S2, Supporting Information) and thus were in direct contact with the metal catalyst during their formation. This implies that, first, large flakes nucleate preferentially at defect sites, and then, surface segregation of carbon stored in the extended defects occurs, resulting in the growth of smaller flakes (sometimes with additional 2 or 3 layers) from below the larger one (**Figure**s 4a,b).

By means of pulsed CVD, the carbon concentration at Cu defect sites is globally reduced, in a way that no segregation takes place, as shown in the schematic picture in Figures 4c,d. The idle step leads to a depletion of the carbon feedstock, and its repetition suppresses the multilayer patches without affecting the graphene quality. This suppression has been found on a large range of the tested parameters (see Figure S3, Supporting Information).

Hydrogen has proven to be necessary during that idle step, probably because of its reducing properties, which help

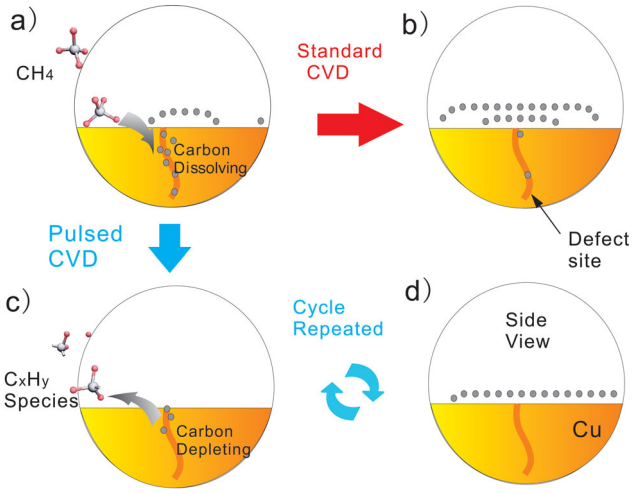

Figure 4. Schematics highlighting the comparison of growth mechanisms near a defect site on copper for a,b) standard CVD, and c,d) pulsed CVD.

depleting the amount of carbon at defects. Note that if the hydrogen flow, besides the methane one, is interrupted during the idle step, the quality of graphene degrades significantly, probably due to copper contamination by impurity gaseous species. However the role of hydrogen during the idle time t_2 is not yet fully understood and further works are needed to elaborate its influence in the patches suppression. Indeed it has been a widely accepted experimental fact[19,31] that hydrogen etches carbon species on Cu. Recently, however, experiments have challenged this common wisdom,[32] and rather point towards the role of gaseous impurities, such as oxygen traces in hydrogen gas, as an etchant of graphene. Even though this alternative scenario would be confirmed, hydrogen is still necessary to neutralize the influence of those contaminants.

5. CVD Pulsed Growth Kinetics

In the case of pulsed growth, only surface-confined growth mode is activated because there is neither carbon segregation, nor storage in copper defects. The smoother edges of graphene domains in pulsed CVD can be understood as that hydrogen not only etches carbon away at the defect sites in Cu, but also at the edges of the already-grown graphene islands. Except for the lowest coordination sites, at corners, the cohesion of graphene, both inside the flake due to the stable carbon sp^2 bonding (≈5.9 eV),[33] and at their edge, presumably due to stabilizing Cu–C bonds, makes the etching of the as-grown graphene a relatively slow process. Thus, an adequate choice of the methane pulse and idle times allows consuming the whole carbon feedstock inside the extended defects in Cu, while only marginally etching the pre-existing graphene flakes. The subsequent methane pulse will then further extend the graphene flake, and so on until full coverage by a single-layer of graphene free of any multilayer patch. Moreover, a good tuning of t_1/t_2 ratio is crucial to achieve exactly one monolayer (Figure S3, Supporting Information), since too long t_1 will let C segregation at defects reappear, while too long t_2 will lead to low coverage of graphene

© 2013 WILEY-VCH Verlag GmbH & Co. KGaA, Weinheim

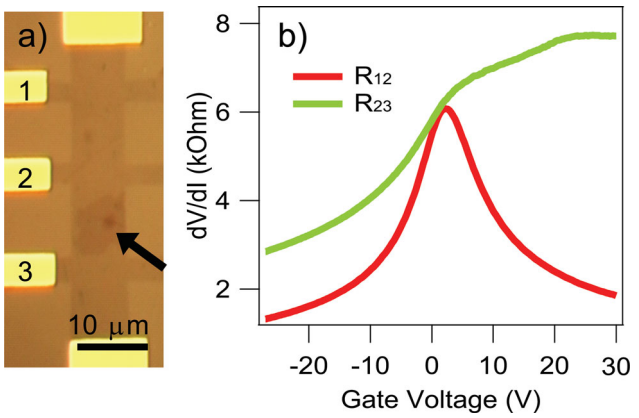

Figure 5. a) Optical image of Hall-bar device made using standard-CVD, with two adjacent regions: zone probed between electrodes 1 and 2 is fully monolayered while zone probed between electrodes 2 and 3 shows a multilayer patch as indicated by the arrow. b) Differential four probe resistance of the two adjacent regions 2–3 (green curve) and 1–2 (red curve) respectively with and without a multi-layer patch.

and prevent formation of continuous films. We found that a "hybrid" process including pulsed injection during the first part of the growth followed by a continuous injection cannot efficiently remove the multilayers patches.

6. Effect of Multilayer Patches for Electron Transport Measurement

In order to further demonstrate the detrimental effect of multilayers on the transport properties of graphene, we have grown graphene with multi-layers based on the standard CVD process on copper foils.[2] Devices such as depicted in **Figure 5**a were fabricated, with two Hall bars on the same graphene grain, using the electron beam lithography followed by an oxygen plasma-etching step. One of them includes a multilayer patch, while the other device serves as a control. We compared the field effect curves (resistance measured while sweeping the back-gate voltage) curves in the two regions.

As can be seen in Figure 5b, the field effect is consistent with what is usually found in monolayer graphene devices for the homogeneous part, whereas a strongly asymmetric and distorted curve is obtained when a zone containing patches is probed (Figure 5a). In that latter measurement, the current has to flow though a multilayered zone. The field effect shows superimposed contributions of the monolayer and the multilayers area together with the resistance of the edges that can lead to *p*–*n* junction like behavior, explaining the asymmetry found in the field effect.[34]

Electronic mobility of samples including one or several multilayers measured at room temperature reproducibly shows a decrease from 5000 to about 1000 $cm^2\ V^{-1}\ s^{-1}$. Furthermore, this reduction of mobility is associated with the appearance of several resistance maxima in the field effect curves, indicating that multilayer patches introduce a significant inhomogeneity in the local doping. One also notices that such multimaxima behavior in field effect becomes more pronounced at lower temperature, and/or when the electrodes get closer to the multilayer patch (Figure S4, Supporting Information). As already discussed in section 3, the top layers are often randomly oriented with respect to the ground one, consistent with results reported elsewhere.[19] It is known that randomly stacked graphene layers do not allow coherent interlayer transport,[35] but sometimes tend to behave as decoupled monolayers with only poor interlayer conduction.[36–39] Therefore, one expects that the multilayer regions are differently doped and thus giving rise to strong fluctuations of the local charge neutrality thus leading to distorted field effect curves such as the one shown in Figure S4, Supporting Information.

As a control experiment, graphene devices made from pulsed-CVD are measured at room temperature on the Si/SiO_2 substrates, showing electronic mobility reaching 6780 $cm^2\ V^{-1}\ s^{-1}$ with a mean value of 5000 $cm^2\ V^{-1}\ s^{-1}$ (see Figure S5, Supporting Information). This proves that the pulsed-CVD technique does not affect the quality of graphene compared to standard growth, as was already suggested by the previously presented Raman analysis.

7. Interest of Pulsed CVD Graphene Applied to Transparent Electrodes

The inhomogeneity in the number of layers has also important consequences on the optical transparency of transferred graphene layers. Indeed, due to quantized optical absorption (see results the literature),[40] in which N-layered regions at patches show optical density increased N times compared to the monolayered zone (at least for $N < 5$, as formed in our patches). In Figure S1 of the Supporting Information, we show that even low density of patches induces strong optical inhomogeneity in stacked layers as the patches are randomly scattered across the sample. We show pulsed-CVD technique provides the opportunity to suppress such "dark spots" for applications in a low-cost and easy-accessible way.

Taking as an example the prospect of using these layers for transparent and flexible electrode applications, which appear as one of the most realistic short-term industrial use of graphene, we have fabricated graphene stacks by repeated transfers on top of each other. Five monolayer-thick stacks exhibit optical transparency comparable to that of ITO-based materials while presenting a superior electronic sheet conductance.[3] Due to the random position of patches, the graphene stacks prepared by standard-CVD further amplifies the filling factor of the multilayer inhomogeneity, resulting in a high density of "dark spots". This effect can be clearly seen in **Figure 6**a–c, in which optical images of full-coverage standard-CVD graphene transferred layer-by-layer (up to three layers) onto oxidized silicon wafers is shown. On the contrary, as shown in Figure 6d–f, homogeneous optical contrast is seen without any multi-layer patch dots for those grown by pulsed-CVD. Notice however some faint lines showing higher contrast, which comes from wrinkles or folds[6] without direct connection to the graphene grain boundaries.[28]

8. Conclusion

We have developed a novel CVD process which allows growing fully homogeneous and continuous graphene strictly

© 2013 WILEY-VCH Verlag GmbH & Co. KGaA, Weinheim

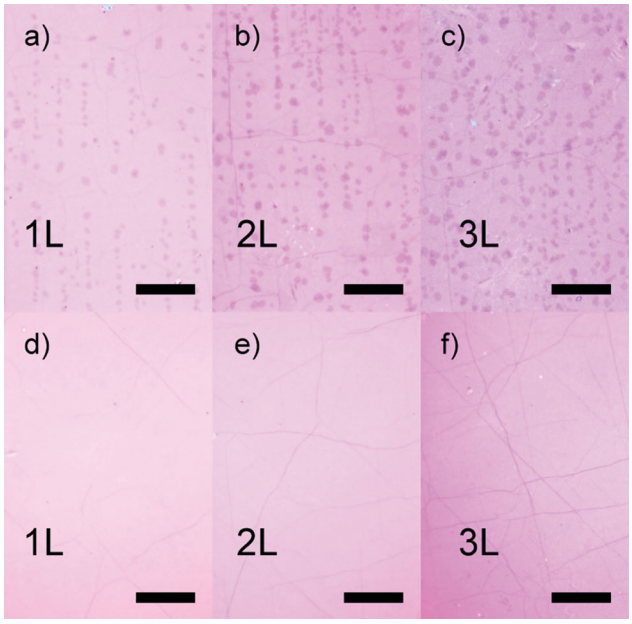

Figure 6. Optical images of the continuous standard a–c) and pulsed d–f) multilayers CVD graphene transferred layer-by-layer (up, 1L, 2L, and 3L referring to one, two, and three stacked layers, respectively) onto oxidized silicon wafers. Scale bars are 50 µm.

monolayered up to the macroscale, and free of multilayer patches which are ubiquitous to standard-CVD on copper foils. This method is based on the repeated pulsed injection of methane, under a constant hydrogen/argon atmosphere. Pulses allow suppressing carbon segregation above the extended defects in bulk Cu.

We have found that the parasitic multilayers in standard-CVD, which were widely overlooked thus far, have noticeable consequences on both the electronic and optical properties of graphene: they reduce the electron mobility, induce local doping, and yield large spatial fluctuations of the optical transparency of graphene. Graphene prepared by pulsed-CVD exhibits high electronic mobility on SiO_2 substrate (mean value of 5000 $cm^2\ V^{-1}\ s^{-1}$) as well as exceptional optical homogeneity from microscopic to macroscopic scales. Pulsed-CVD is a versatile technique which can be readily implemented in CVD reactors employed routinely in graphene research, under a broad range of pressure conditions, and presumably also on a variety of substrates for graphene growth (e.g., Pt, Ni). This is a scalable technique allowing "vacuuming" multilayer graphene patches that are usually "hidden under the carpet". It further enables precise monolayer-by-monolayer engineering for emerging applications such as physical layer deposition of graphene heterostructures.

9. Experimental Section

Cu foil (25 µm-thick) of 99.8% purity (Alfa-Aesar) was used in the CVD process. A home-made CVD reactor with an 80 mm diameter quartz tube and an effective uniform heating length of about 10 cm is used. Temperature is kept constant with the 3-zone split furnace. All components are controlled by a home-made program, which enables real-time control of the flow rates with the help of the electronic mass-flow controller. Full automatization allows independent PID controls of reactor pressure (by adjustment of screw pump speed) and temperature. Cu foils are loaded into the CVD reactor after acetone cleaning, followed by hydrogen annealing at 1000 °C. For safety reasons, hydrogen is diluted in Ar at 10%. In standard-CVD, at the dendritic regime, partial pressures of CH_4 and H_2 are 2.8 µbar, and 0.1 mbar, respectively, while the values are 50 µbar CH_4 and 25 mbar H_2 for the hexagonal regime. The partial pressures are kept the same for pulsed-CVD at both regimes. Optimized pulse durations t_1/t_2 are 10 s/50 s and 5 s/55 s, for dendritic and hexagonal regimes, respectively. Graphene grown on Cu is then transferred by a PMMA-assisted method, as reported elsewhere.[2] The Cu etchant was 0.1 g/mL $(NH_4)_2S_2O_8$, with about 2 h etching time. Graphene devices fabricated by standard electron beam lithography are contacted with Ti (5 nm)/Au (50nm) electrodes for carrying out electron transport measurements.

Supporting Information

Supporting Information is available from the Wiley Online Library or from the author.

Acknowledgements

The authors are indebted to C. Guttin, J. Jarreau, and R. Haettel for their help and technical support. The authors appreciate the help from NanoFab team of the Néel Institute. This work is partially supported by the contracts ANR-2010-BLAN-SUPERGRAPH and ANR-11-NANO-0025 TRI-CO, the EU contract NMP3-SL-2010–246073 GRENADA, ERC, CNRS DEFI Nano and the Nanosciences Foundation of Grenoble. Z.H. acknowledges the PhD grant ADR from the Région Rhône-Alpes CIBLE program.

Received: May 21, 2013
Revised: July 30, 2013
Published online: October 24, 2013

[1] K. S. Novoselov, V. I. Falko, L. Colombo, P. R. Gellert, K. K. M. G. Schwab, *Nature* **2012**, *490*, 192.
[2] X. Li, W. W. Cai, J. An, S. Kim, J. Nah, D. Yang, R. Piner, A. Velamakanni, I. Jung, E. Tutuc, S. K. Banerjee, L. Colombo, R. S. Ruoff, *Science* **2009**, *324*, 5932.
[3] S. Bae, H. K. Kim, Y. B. Lee, X. F. Xu, J. S. Park, Y. Zheng, J. Balakrishnan, T. Lei, H. R. Kim, Y. I. Song, Y. J. Kim, K. S. Kim, B. Özyilmaz, J. H. Ahn, B. H. Hong, S. Iijima, *Nat. Nanotechnol.* **2010**, *5*, 574.
[4] G. Xu, Y. Zhang, X. Duan, A. A. Balandin, K. L. Wang **2013**, arXiv:1302.3922.
[5] G. X. Ni, Y. Zheng, S. Bae, H. R. Kim, A. Pachoud, Y. S. Kim, C. L. Tan, D. Im, J. H. Ahn, B. H. Hong, B. Özyilmaz, *ACS Nano* **2012**, *6*, 1158.
[6] W. Zhu, T. Low, V. Perebeinos, A. A. Bol, Y. Zhu, H. Yan, J. Terso, P. Avouris, *Nano Lett.* **2012**, *12*, 3431.
[7] V. E. Calado, G. F. Schneider, A. M. M. G. Theulings, C. Dekker, L. M. K. Vandersypen, *Appl. Phys. Lett.* **2012**, *101*, 103116.
[8] Q. K. Yu, L. A. Jauregui, W. Wu, R. Colby, J. Tian, Z. H. Su, H. L. Cao, Z. Z. Liu, D. Pandey, D. G. Wei, T. F. Chung, P. Peng, N. P. Guisinger, E. A. Stach, J. M. Bao, S. S. Pei, Y. P. Chen, *Nat. Mater.* **2011**, *10*, 443.
[9] L. Gao, W. Ren, H. Xu, L. Jin, Z. Wang, T. Ma, L.-P. Ma, Z. Zhang, Q. Fu, L.-M. Peng, X. Bao, H.-M. Cheng, *Nat. Commun.* **2012**, *3*, 699.

© 2013 WILEY-VCH Verlag GmbH & Co. KGaA, Weinheim

[10] Z. Yan, J. Lin, Z. Peng, Z. Sun, Y. Zhu, L. Li, C. Xi-ang, E. L. Samuel, C. Kittrell, J. M. Tour, *ACS Nano* **2012**, *6*, 9110.
[11] K. Yan, H. Peng, Y. Zhou, H. Li, Z. Liu, *Nano Lett.* **2011**, *11*, 1106.
[12] B. S. Hu, H. Ago, Y. Ito, K. Kawahara, M. Tsuji, E. Magome, K. Sumitani, N. Mizuta, K. Ikeda, S. Mizuno, *Carbon* **2012**, *50*, 57.
[13] C. Hwang, K. Yoo, S. J. Kim, E. K. Seo, H. Yu, L. P. Biró, *J. Phys. Chem. C* **2011**, *115*, 22369.
[14] X. Li, C. W. Magnuso, A. Venugopal, R. M. Tromp, J. B. Hannon, E. M. Vogel, L. Colombo, Rodney S. Ruoff, *J. Am. Chem. Soc.* **2011**, *133*, 2816.
[15] N. Petrone, C. R. Dean, I. Meric, A. M. van der Zande, P. Y. Huang, L. Wang, D. Muller, K. L. Shepard, J. Hone, *Nano Lett.* **2012**, *12*, 2751.
[16] M. Massicotte, V. Yu, E. Whiteway, D. Vatnik, M. Hilke, **2013**, arXiv:1301.7033.
[17] G. H. Han, F. Güneş, J. J. Bae, E. S. Kim, S. J. Chae, H.-J. Shin, J.-Y. Choi, D. Pribat, Y. H. Lee, *Nano Lett.* **2011**, *11*, 4144.
[18] Y. Zhang, L. Zhang, P. Kim, M. Ge, Z. Li, C. Zhou, *Nano Lett.* **2012**, *12*, 2810.
[19] I. Vlassiouk, M. Regmi, P. Fulvio, S. Dai, P. Datskos, G. Eres, S. Smirnov, *ACS Nano* **2011**, *5*, 6069.
[20] Z. Luo, S. Kim, N. Kawamoto, A. M. Rappe, A. T. C. Johnson, *ACS Nano* **2011**, *5*, 9154.
[21] P. Venezuela, M. Lazzeri, F. Mauri, *Phys. Rev. B* **2011**, *84*, 035433.
[22] Y. Hao, Y. Wang, L. Wang, Z. Ni, Z. Wang, R. Wang, C. K. Koo, Z. Shen, J. T. L. Thong, *Small* **2010**, *6*, 195.
[23] A. Ya. Tontegode et al., *Progr. Surf. Sci.* **1991**, *38*, 429.
[24] J. Oudar, H. Wise, *Deactivation and Poisoning of Catalysts*, Dekker, New York **1985**.
[25] J. B. Butt, E. E. Petersen, *Activation, deactivation, and poisoning of catalysts*, Academic Press, Inc., San Diego, CA **1988**.
[26] E. V. Rut'kov, N. R. Gall, *Physics and applications of graphene experiments* (Ed: S. Mikhailov), Ch. 11, InTech, Rijeka, Croatia **2011**.
[27] R. B. McLellan, *Mater. Sci. Eng.* **1972**, *9*, 121140.
[28] X. S. Li, W. W. Cai, L. Colombo, R. S. Ruoff, *Nano Lett.* **2009**, *9*, 4268.
[29] S. Nie, W. Wu, S. Xing, Q. Yu, J. Bao, S. Pei, K. F. McCarty, *New J. Phys.* **2012**, *14*, 093028.
[30] C.-Y. Su, A.-Y. Lu, C.-Y. Wu, Y.-T. Li, K.-K. Liu, W. Zhang, S.-Y. Lin, Z.-Y. Juang, Y.-L. Zhong, F.-R. Chen, L.-J. Li, *Nano Lett.* **2011**, *11*, 3612.
[31] Y. Zhang, Z. Li, P. Kim, L. Zhang, C. Zhou, *ACS Nano* **2012**, *6*, 126.
[32] S. Choubak, M. Biron, P. L. Levesque, R. Martel, P. Desjardin, *J. Phys. Chem. Lett.* **2013**, *4*, 1100.
[33] M. C. Schabel, J. L. Martins, *Physics Rev. B* **1992**, *46*, 7185.
[34] H. Y. Chiu, V. Perebeinos, Y.-M. Lin, P. Avouris, *Nano Lett.* **2010**, *10*, 4634.
[35] Y. Kim, H. Yun, S.-G. Nam, M. Son, D. S. Lee, D. C. Kim, S. Seo, H. C. Choi, H.-J. Lee, S. W. Lee, J. S. Kim, **2012**, arXiv: 1206.3410.
[36] B. Wang, M.-L. Bocquet, *Nanoscale* **2012**, *4*, 4687.
[37] O. Taisuke, A. Bostwick, J. L. McChesney, T. Seyller, K. Horn, E. Rotenberg, *Phys. Rev. Lett.* **2007**, *98*, 206802.
[38] J. Hass, F. Varchon, J. E. Millan-Otoya, M. Sprinkle, N. Sharma, W. A. de Heer, C. Berger, P. N. First, L. Magaud, E. H. Conrad, *Phys. Rev. Lett.* **2008**, *100*, 125504.
[39] E. J. Mele, *J. Phys. D: Appl. Phys.* **2012**, *45*, 154004.
[40] R. R. Nair, P. Blake, A. N. Grigorenko, K. S. Novoselov, T. J. Booth, T. Stauber, N. M. R. Peres, A. K. Geim, *Science* **2008**, *320*, 1308.

© 2013 WILEY-VCH Verlag GmbH & Co. KGaA, Weinheim